



1 **Analysing surface energy balance closure and partitioning**  
2 **over a semi-arid savanna FLUXNET site in Skukuza, Kruger**  
3 **National Park, South Africa**  
4

5 Nobuhle P. Majazi<sup>1,2</sup>, Chris M. Mannaerts<sup>2</sup>, Abel Ramoelo<sup>1</sup>, Renaud Mathieu<sup>1,3</sup>, Alecia  
6 Nickless<sup>4</sup>, Wouter Verhoef<sup>2</sup>

7 <sup>1</sup>Earth Observation Group, Natural Resources and Environment, Council for Scientific and Industrial Research,  
8 Pretoria, South Africa, 0001

9 <sup>2</sup>Department of Water Resources, Faculty of Geo-Information Science and Earth Observation (ITC), University  
10 of Twente, Enschede, 75AA, the Netherlands

11 <sup>3</sup>Department of Geography, Geoinformatics and Meteorology, University of Pretoria, South Africa

12 <sup>4</sup>Nuffield Department of Primary Care Health Sciences, University of Oxford, Oxford, OX2 6GG, United  
13 Kingdom

14 *Correspondence to:* N. P. Majazi ([nmajazi@csir.co.za](mailto:nmajazi@csir.co.za))  
15

16 **Abstract:** Flux tower data are in high demand to provide essential terrestrial climate, water and radiation budget  
17 information needed for environmental monitoring and evaluation of climate change impacts on ecosystems and  
18 society in general. They are also intended for calibration and validation of satellite-based earth observation and  
19 monitoring efforts, such as for example assessment of evapotranspiration from land and vegetation surfaces  
20 using surface energy balance approaches.

21 Surface energy budget methods for ET estimation rely to a large extent on the basic assumption of a  
22 surface energy balance closure, assuming the full conversion of net solar radiation reaching the land surface into  
23 soil heat conduction and turbulent fluxes, i.e. the sensible (or convection) and latent heat components of the  
24 energy balance.

25 In this paper, the Skukuza flux tower data were analysed in order to verify their use for validation of  
26 satellite-based evapotranspiration methods, under development in South Africa. Data series from 2000 until  
27 2014 were used in the analysis. The energy balance ratio (EBR) concept, defined as the ratio between the sum of  
28 the turbulent convective and latent heat fluxes and radiation minus soil heat was used. Then typical diurnal  
29 patterns of EB partitioning were derived for four different seasons, well illustrating how this savannah-type  
30 biome responds to weather conditions. Also the particular behaviour of the EB components during sunrise and  
31 sunset conditions, being important but usually neglected periods of energy transitions and inversions were noted  
32 and analysed.

33 Annual estimates and time series of the surface energy balance and its components were generated, including an  
34 evaluation of the balance closure. The seasonal variations were also investigated as well as the impact of  
35 nocturnal observations on the overall EB behaviour.  
36

37 **1 Introduction**

38 The net solar radiation ( $R_n$ ) reaching the earth's surface determines the amount of energy available for  
39 transformation into energy balance components, i.e. latent (LE), sensible (H) and ground (G) heat fluxes,  
40 including heat stored by the canopy and the ground. Energy partitioning on the earth's surface is a function of  
41 interactions between biogeochemical cycling, plant physiology, the state of the atmospheric boundary layer and  
42 climate (Wilson et al., 2002). How the turbulent fluxes (sensible and latent heat fluxes) are partitioned in an  
43 ecosystem plays a critical role in determining the hydrological cycle, boundary layer development, weather and  
44 climate (Falge et al., 2005). Understanding the partitioning of energy, particularly the turbulent fluxes, is  
45 important for water resource management in (semi) arid regions, where potential evapotranspiration far exceeds  
46 precipitation.

47 Eddy covariance (EC) systems are currently the most reliable method for measuring carbon, energy and  
48 water fluxes, and they have become a standard technique in the study of surface-atmosphere boundary layer  
49 interactions. Hence, they provide a distinct contribution to the study of environmental, biological and



50 climatological controls of the net surface exchanges between the land surface (including vegetation) and the  
51 atmosphere (Aubinet, et al., 1999; Baldocchi et al., 2001). The accuracy of these data is very important because  
52 they are used to validate and assess performance of land surface and climate models. However, the eddy  
53 covariance techniques have limitations in terms of data processing and quality control methods, especially under  
54 complex conditions (e.g., unfavorable weather, such as high turbulence and low wind speed, and heterogeneous  
55 topography). In EC measurements, the ideal situation is that available energy, i.e. net radiation minus soil heat  
56 flux is equal to the sum of the turbulent fluxes (latent and sensible heat fluxes) ( $R_n - G = LE + H$ ); however, in  
57 most instances, the available energy (i.e. net radiation–soil heat flux ( $R_n - G$ )) is larger than the sum of the  
58 measurable turbulent fluxes of sensible heat and latent heat. Extensive research investigated and reported the  
59 issue of surface energy imbalance in EC observations (Barr et al., 2012; Chen et al., 2009; Foken et al., 2010;  
60 Franssen et al., 2010; Mauder et al., 2007), and this closure error (or imbalance) has been documented to be  
61 around 10-30 %. Causes for non-closure include unaccounted soil and canopy heat storage, non-inclusion of the  
62 low frequency turbulence in the computation of the turbulent fluxes, land surface heterogeneities, systematic  
63 measurement and sampling errors. This imbalance has implications on how energy flux measurements should be  
64 interpreted and how these estimates should be compared with model simulations. The surface energy balance  
65 closure is an accepted validation procedure of eddy covariance data quality (Twine et al., 2000; Wilson et al.,  
66 2002), and different methods have been used to assess the energy closure and partitioning, including ordinary  
67 least squares regression (OLS) method, the residual method, i.e.  $Residual = R_n - G - H - LE$ , and the energy balance  
68 ratio, i.e.  $EBR = LE + H / R_n - G$ .

69 Several researchers have investigated surface energy partitioning and energy balance closure for  
70 different ecosystems, including savannas. Bagayoko et al. (2007) examined the seasonal variation of the energy  
71 balance in West African savannas, and noted that latent heat flux played a major role in the wet season, whereas  
72 sensible heat flux was significant in the dry season. In the grassland Mongolian Plateau, Li et al. (2006)  
73 concluded that sensible heat flux dominated the energy partitioning, followed by ground heat flux, even during  
74 the rainy season, which showed a slight increase in latent heat flux. Gu et al. (2006) used different ratios  
75 (Bowen ratio,  $G/R_n$ ,  $H/R_n$  and  $LE/R_n$ ) to investigate surface energy exchange in the Tibetan Plateau, and  
76 showed that during the vegetation growth period,  $LE$  was higher than  $H$ , and this was reversed during the post-  
77 growth period.

78 Research on the South African savanna, i.e. using data from the Skukuza EC system, has focused mainly on  
79 the carbon exchange, fire regimes, and in global analysis of the energy balance (Archibald et al., 2009; Kutsch  
80 et al., 2008; Williams et al., 2009). Hence, the need to explore the surface energy partitioning and energy  
81 balance closure of this ecosystem. In this study, we will examine the surface energy balance partitioning into  
82 soil heat conduction, convection (sensible) and latent heat components and its energy balance closure using 15  
83 years (2000-2014) of eddy covariance data from the Skukuza flux station.

84 First, a multi-year surface energy balance closure analysis was done, and annual values for the EB  
85 components derived, including an evaluation of the balance closure and its error sources. To further investigate  
86 the EB partitioning and closure at this location and biome, the seasonal effect on the EB variations was also  
87 assessed. Thirdly, the effect of nocturnal (nighttime) observations on the overall daily EBR was verified. Then  
88 the partitioning of the net solar radiation into soil heat and the turbulent fluxes ( $L + HE$ ) during the different



89 seasons was assessed at the sub-daily (30-min) scale for this African savanna system for the year 2012 with  
90 meteorological data.

91

## 92 **2 Materials and methods**

### 93 **2.1 Site description**

94 The Skukuza flux tower (25.02°S, 31.50°E) was established early 2000 as part of the SAFARI 2000 campaign  
95 and experiment, set up to understand the interactions between the atmosphere and the land surface in southern  
96 Africa by connecting ground data of carbon, water, and energy fluxes with remote sensing data generated by  
97 Earth observing satellites (Scholes et al., 2001; Shugart et al., 2004).

98 The site is located in the Kruger National Park (South Africa) at 365 m above sea level, and receives  
99  $550 \pm 160$  mm precipitation per annum between November and April, with significant inter-annual variability.  
100 The year is divided into a hot, wet growing season and a warm, dry non-growing season. The soils are generally  
101 shallow, with coarse sandy to sandy loam textures (about 65 % sand, 30 % clay and 5% silt). The area is  
102 characterised by a catenal pattern of soils and vegetation, with broad-leaved *Combretum* savanna on the crests  
103 dominated by the small trees (*Combretum apiculatum*), and fine-leaved *Acacia* savanna in the valleys dominated  
104 by *Acacia nigrescens* (Scholes et al., 1999). The vegetation is mainly open woodland, with approximately 30 %  
105 tree canopy cover of mixed *Acacia* and *Combretum* savanna types. Tree canopy height is 5–8 m with occasional  
106 trees (mostly *Sclerocarya birrea*) reaching 10 m. The grassy and herbaceous understory comprises grasses such  
107 as *Panicum maximum*, *Digitaria eriantha*, *Eragrostis rigidior*, and *Pogonarthria squarrosa*.

108

#### 109 **2.1.1 Eddy covariance system**

110 Since 2000, ecosystem-level fluxes of water, heat and carbon dioxide are measured using an eddy covariance  
111 system mounted at 17 m height of the 22 m high flux tower. The measurements taken and the instruments used  
112 are summarised in Table 1.

113

#### 114 **(Table 1)**

115

116 From 2000 to 2005, H and LE were derived from a closed-path CO<sub>2</sub>/H<sub>2</sub>O monitoring system, which was  
117 replaced by the open-path gas analyser in 2006. Also, from 2000 to 2008, incident and reflected shortwave  
118 radiation (i.e. 300–1100 nm, Wm<sup>-2</sup>), incident and reflected near-infrared (600–1100 nm, Wm<sup>-2</sup>) and incoming  
119 and emitted longwave radiation (>3.0 μm, Wm<sup>-2</sup>) measurements were made using a two-component net  
120 radiometer (Model CNR 2: Kipp & Zonen, Delft, The Netherlands) at 20 s intervals and then recorded in the  
121 data-logger as 30 min averages; this was replaced with the Kipp & Zonen NRLite net radiometer in 2009.

122 Ancillary meteorological measurements include air temperature and relative humidity, also measured at  
123 16 m height, using a Campbell Scientific HMP50 probe; precipitation at the top of the tower using a Texas  
124 TR525M tipping bucket rain gauge; wind speed and direction using a Climatronics Wind Sensor; and soil  
125 temperature using Campbell Scientific 107 soil temperature probe.

126

127 **2.1.2 Data pre-processing**

128 Post-processing of the raw high frequency (10 Hz) data for calculation of half-hour periods of the turbulent  
129 fluxes of sensible heat ( $H$ ;  $W m^{-2}$ ), water vapor ( $LE$ ;  $W m^{-2}$ ), and  $CO_2$  ( $F_c$ ;  $g CO_2 m^{-2} time^{-1}$ ) involved standard  
130 spike filtering, planar rotation of velocities and lag correction to  $CO_2$  and  $q$  (Aubinet et al., 1999; Wilczak et al.,  
131 2001). All fluxes are reported as positive upward from the land to the atmosphere. Frequency response  
132 correction of some of the energy lost due to instrument separation, tube attenuation, and gas analyzer response  
133 for  $LE$  and  $F_c$  was performed with empirical cospectral adjustment to match the  $H$  co-spectrum (Eugster and  
134 Senn, 1995; Su et al., 2004).

135

136 **2.2 Data analysis**

137 Half-hourly measurements of eddy covariance and climatological data from 2000 to 2014 were used to assess  
138 surface energy partitioning and closure. Screening of the half-hourly data rejected i) data from periods of sensor  
139 malfunction (i.e. when there was a faulty diagnostic signal), (ii) incomplete 30 minute datasets of net radiation,  
140 ground, latent and sensible heat fluxes, and iii) outliers. After data screening, flux data with non-missing values  
141 of net radiation ( $R_n$ ), ground heat flux ( $G$ ), latent heat ( $LE$ ) flux and sensible heat flux ( $H$ ) data were arranged  
142 according to monthly and seasonal periods (summer (December – February), autumn (March – May), winter  
143 (June – August), and spring (September – November)), as well as into daytime and nighttime. These data  
144 without gaps were then used to analyse for surface energy balance closure.

145

146 **2.2.1 Surface energy balance assessment**

147 The law of conservation of energy states that energy can neither be created nor destroyed, but is transformed  
148 from one form to another, hence the ideal surface energy balance equation is written as:

$$149 \quad R_n - G = H + LE \quad (1)$$

150 Energy imbalance occurs when both sides of the equation do not balance. The energy balance closure was  
151 evaluated for at different levels, i.e. multi-year, seasonal, and day/ night periods, using two methods, i.e.

152 i) The ordinary least squares method (OLS), which is the regression between turbulent fluxes (right side  
153 of equation 1,  $H+LE$ ) and available energy (left side of equation 1,  $R_n-G$ )

154 Ideal closure is when the intercept is zero and slope and the coefficient of determination are one. This method is  
155 only valid when there are no random errors in the independent variables, i.e.  $R_n$  and  $G$ .

156 ii) The energy balance ratio (EBR), i.e. ratio of the sum of turbulent fluxes to the available energy

$$157 \quad EBR = \frac{\sum(H+LE)}{\sum(R_n-G)} \quad (2)$$

158 The EBR gives an overall evaluation of energy balance closure at longer time scales by averaging over random  
159 errors in the half-hour measurements; and the ideal closure is 1. EBR has the potential to neglect biases in the  
160 half-hourly data, such as the tendency to overestimate positive fluxes during the day and underestimate negative  
161 fluxes at night.

162



163 **2.2.2 Analysing surface energy partitioning**

164 To evaluate solar radiation variation and partitioning into latent and sensible heat fluxes in this biome, EC  
165 surface energy data from 2000 to 2014 were used. The data gaps in these data were first filled using the Amelia  
166 II software (Honaker, King, & Blackwell, 2011). This R-program was designed to impute missing data using a  
167 bootstrapping-based multiple imputation algorithm. The minimum, maximum and mean statistics of Rn, H, LE  
168 and G were then estimated.

169 To further investigate how meteorological data influence and/or affect the partitioning of the surface  
170 energy fluxes, meteorological variables (temperature, precipitation and soil moisture) from 2012 were analysed.  
171 The monthly and seasonal variations of energy partitioning were investigated, as well as the energy flux  
172 inversions during night-day transitions.

173

174 **3 Results and discussion**

175 **3.1 Surface energy balance assessment**

176 Data completeness varied largely between 12.76 % (2001) and 57.65 % (2010), with a mean of 36 % and  
177 standard deviation 15 %. The variation in data completeness is due to a number of factors including instrument  
178 failures, changes and (re)calibration, and poor weather conditions.

179

180 **3.1.1 Multi-year analysis of surface energy balance closure**

181 Fig 1 summarises results of the multi-year energy balance closure analysis for the Skukuza eddy covariance  
182 system from 2000 to 2014. The slopes ranged between 0.93 and 1.47, with a mean  $1.19 \pm 0.21$ , and the  
183 intercepts were a mean of  $17.79 \pm 32.96 \text{ Wm}^2$ .  $R^2$  ranged between 0.73 in 2005 and 0.92 in 2003, with a mean  
184 of 0.86 with standard deviation of 0.05.

185 The annual energy balance ratio (EBR) ranged between 0.44 in 2007 and 3.76 in 2013, with a mean of  
186  $0.97 \pm 0.81$ . Between 2004 and 2008, EBR ranges between 0.44 and 0.53, whereas from 2000 to 2003 and 2009  
187 to 2014, the EBR ranged 0.76 and 1.09, with 2013 having an extreme EBR of 3.76. The EBR for 2010 to 2012  
188 were greater than 1, indicating an overestimation of the turbulent fluxes (H+LE) compared to the available  
189 energy. The remaining years were less than 1, indicating that the turbulent fluxes were lower than the available  
190 energy. The period of low EBR between 2004 and 2008 is characterised by the absence of negative values of  
191 available energy (Rn-G, i.e. the nocturnal measurements of fluxes and radiation) as illustrated in Fig 1. Our final  
192 proposed mean annual EBR estimate for the (2000-2014) 15-year period, excluding those with data issues  
193 (2004 to 2008, and 2013), was therefore 0.93 with standard deviation of 0.11.

194 **(Figure 1)**

195 The EBR results for the Skukuza eddy covariance system, with a mean of 0.93 (only the years with good data  
196 quality), are generally within the reported accuracies by most studies that report the energy balance closure error  
197 at 10 – 30%. Chen et al. (2009) report a mean of 0.98 EBR, average slope of 0.83, and  $R^2$  ranges between 0.87  
198 and 0.94 for their study in the semi-arid region of Mongolia. Wilson et al., (2002) also reported that the mean  
199 annual EBR for 22 FLUXNET sites was 0.84, ranging from 0.34 to 1.69, and slopes and intercepts ranging from  
200 0.53 to 0.99, and from  $-33$  to  $37 \text{ W m}^{-2}$ , respectively. Yuling et al. (2005) also report that in the ChinaFLUX,



201 EBR ranged between 0.58 and 1.00, with a mean of 0.83. von Randow et al. (2004) showed an energy  
202 imbalance of 26 % even after correcting for the angle of attack on the sonic anemometer in the forested Jeru  
203 study area in the Amazon, and explained this as due to either slow wind direction changes which result in low  
204 frequency components that cannot be captured using short time rotation scales, and the difficulty in estimating  
205 horizontal flux divergences caused by energy that is transported horizontally by circulations. Sanchez et al.,  
206 (2010) showed that the inclusion of the storage term in the EBR improved the closure by almost 6 % from 0.72,  
207 in their study in a FLUXNET boreal site in Finland. Using data from the Tibetan Observation and Research  
208 Platform (TORP), Liu et al. (2011) observed an EBR value of 0.85 in an alfalfa field in semi-arid China. Also  
209 under similar semi-arid conditions, in China, an EBR value of 0.80 was found by Xin and Liu (2010) in a maize  
210 crop. Were et al. (2007) reported EBR values of about 0.90 over shrub and herbaceous patches, in a dry valley  
211 in southeast Spain.

212

### 213 3.1.2 Seasonal variation of EBR

214 Fig 2 shows the seasonal OLS results for the combined 15 year period. The slopes ranged between 0.99 and  
215 1.28, with a mean of  $1.17 \pm 0.13$ , and the intercepts were a mean of  $25.54 \text{ Wm}^{-2} \pm 10.77 \text{ Wm}^{-2}$ .  $R^2$  ranged  
216 between 0.73 and 0.82 with a mean of  $0.78 \pm 0.05$ . The EBR for the different seasons ranged between 0.50 and  
217 0.88, with a mean of 0.7. The winter season had the lowest EBR of 0.50, while the summer season had the  
218 highest EBR of 0.88, autumn and spring had EBR of 0.68 and 0.74, respectively.

#### 219 (Figure 2)

220 Wilson et al. (2002) comprehensively investigated the energy closure of the summer and winter seasons for 22  
221 FLUXNET sites for 50 site-years. They also reported higher energy balance correlation during the summer  
222 compared to the winter season, with the mean  $R^2$  of 0.89 and 0.68, respectively. However, their EBR showed  
223 smaller differences between the two seasons, being 0.81 and 0.72, for summer and winter, respectively, whereas  
224 for Skukuza, the differences were much significant. Ma et al. (2009) reported an opposite result from the  
225 Skukuza results, showing energy closures of 0.70 in summer and 0.92 in winter over the flat prairie on the  
226 northern Tibetan Plateau.

227

### 228 3.1.3 Day – night-time effects

229 Fig 3 shows the daytime and nocturnal OLS regression results for the 15 year period. The daytime and nocturnal  
230 slopes were 0.99 and 0.11, with the intercepts being  $76.76$  and  $1.74 \text{ Wm}^{-2}$ , respectively. Daytime and nocturnal  
231  $R^2$  were 0.64 and 0.01, respectively. The EBR for the different times of day were 0.72 and -4.59, daytime and  
232 nocturnal, respectively.

233

#### 234 (Figure 3)

235

236 Results from other studies also reported a higher daytime surface energy balance closure. For instance, Wilson  
237 et al., (2002) show that the mean annual daytime energy closure was 0.8, whereas the nocturnal EBR was  
238 reported to be negative or was much less or much greater than 1.



239 The large nocturnal energy imbalances are explained to be a result of low friction velocity, which leads to weak  
240 turbulence. Lee and Hu (2002) hypothesized that the lack of energy balance closure during nocturnal periods  
241 was often the result of mean vertical advection, whereas Aubinet et al., (1999) and Blanken et al., (1997)  
242 showed that the energy imbalance during nocturnal periods is usually greatest when friction velocity is small.

243

### 244 3.2 Surface energy partitioning

#### 245 3.2.1 Surface energy measurements

246 The daily mean measurements of the energy budget components from 2000 to 2014 are highlighted in Fig 4.  
247 The seasonal cycle of each component can be seen throughout the years, where at the beginning of each year the  
248 energy budget components are high, and as the each year progresses they all decrease to reach a low during the  
249 middle of the year, which is the winter season. The multi-year daily means of  $R_n$ ,  $H$ ,  $LE$  and  $G$  were  $139.1 \text{ Wm}^{-2}$   
250  $^2$ ,  $57.70 \text{ Wm}^{-2}$ ,  $42.81 \text{ Wm}^{-2}$  and  $2.94 \text{ Wm}^{-2}$ , with standard deviations of  $239.75 \text{ Wm}^{-2}$ ,  $104.15 \text{ Wm}^{-2}$ ,  $70.58 \text{ Wm}^{-2}$   
251 and  $53.67 \text{ Wm}^{-2}$ , respectively.

252 (Figure 4)

253

#### 254 3.2.2 Influence of weather conditions and seasonality

255 In arid/semi-arid ecosystems, solar radiation is not a limiting factor for evapotranspiration, instead it is mainly  
256 limited by water availability. The seasonal fluctuations of energy fluxes are affected by the seasonal changes in  
257 the solar radiation, air and soil temperatures, and soil moisture (Baldocchi et al., 2000; Arain et al., 2003). These  
258 climatic variables influence vegetation dynamics in an ecosystem, as well as how solar radiation is partitioned.  
259 Hence, daily measurements of precipitation, soil moisture and air temperature for 2012 were evaluated to  
260 investigate the partitioning of the surface energy in the semi-arid landscape of Skukuza.

261 Fig 5 presents daily averages of air temperature, soil water content and total precipitation for Skukuza  
262 for 2012. The total annual precipitation was 534.24 mm, distributed from September and April, with the highest  
263 monthly amount of 148.59 mm recorded in January. Soil water content ranged between 5.23 and 26.4 %, and  
264 soil temperature varied between 18 and 30 °C. The mean daily air temperature shows some variability between  
265 months, ranging between 9 and 32 °C, with the mean annual air temperature being 26 °C.

266 (Figure 5)

267 To illustrate the partitioning of solar radiation into the different fluxes throughout the year, Fig 6 presents the  
268 multi-year mean monthly variations of the surface energy components. showing a general decrease of the  
269 components between February and June, which then gradually increases again until November. The multi-year  
270 monthly means of  $R_n$ ,  $H$ ,  $LE$  and  $G$  were  $97.48 \text{ Wm}^{-2}$  (June) and  $200.41 \text{ Wm}^{-2}$  (February),  $34.59 \text{ Wm}^{-2}$  (June)  
271 and  $76.80 \text{ Wm}^{-2}$  (February),  $7.06 \text{ Wm}^{-2}$  (July) and  $104.02 \text{ Wm}^{-2}$  (January),  $-2.91 \text{ Wm}^{-2}$  and  $21.55 \text{ Wm}^{-2}$   
272 (September), respectively.

273 (Figure 6)

274 The higher monthly means of net radiation during the months of November and February as compared to those  
275 of December and January is due to the presence of clouds and the fact that December and January are the





276 months of peak precipitation in the region (Scholes et al., 2001). Net radiation is affected by surface albedo,  
277 presence of cloud and water vapour (Goosse et al., 2008).

278 Fig 7 illustrates the averaged diurnal variations of the surface energy balance components for the four  
279 seasons (summer, autumn, winter and spring). The general trend reveals that sensible heat flux dominated the  
280 energy partitioning during three seasons, followed by latent heat flux, and lastly the soil heat flux, except during  
281 the summer season where latent heat flux was larger than sensible heat flux. This period is characterised by high  
282 incoming solar radiation, as illustrated by the high midday net radiation of between 700 and 800  $\text{Wm}^{-2}$ , and high  
283 precipitation (Fig 5). Autumn (Fig 7b) is characterised by reduced net radiation, as shown by midday net  
284 radiation of around 500  $\text{Wm}^{-2}$ , whereas winter (Fig 7c) had the lowest midday net radiation, and minimum latent  
285 heat flux.

286 **(Figure 7)**

287 Just before the first rains, i.e. between September and November, tree flowering and leaf emergence occurs in  
288 the semi-arid savanna in the Skukuza area (Archibald and Scholes, 2007), and grasses shoot as soil moisture  
289 availability improves with the rains (Scholes et al., 2003). This is characterised by a gradual increase in latent  
290 heat flux (evapotranspiration), which, when compared to the winter season, is significantly lower than the  
291 sensible heat flux, as illustrated in Fig 5 and 7. As the rainy season progresses, and vegetation development  
292 peaks, latent heat flux also reaches its maximum, becoming significantly higher than sensible heat flux. Between  
293 March and September, when leaf senescence occurs, the leaves gradually change colour to brown and grass to  
294 straw, and trees defoliate, sensible heat flux again gradually becomes significantly higher than LE, as illustrated  
295 in Fig 7b-d.

296 Gu et al. (2006) examined how soil moisture, vapour pressure deficit (VPD) and net radiation control  
297 surface energy partitioning. They ascertained that with ample soil moisture, latent heat flux dominates over  
298 sensible heat flux, and reduced soil moisture availability reversed the dominance of latent heat over sensible  
299 heat, because of its direct effect on stomatal conductance. An increase in net radiation, on the other hand, also  
300 increases both sensible and latent heat fluxes. The increase of either then becomes a function of soil moisture  
301 availability, since they cannot increase in the same proportion. Gu et al., (2006) also revealed that the  
302 relationship between net radiation and latent heat flux is convex, while that of net radiation and sensible heat  
303 flux is concave. Their findings are consistent with our results, which show that during the rainy season, latent  
304 heat flux was significantly higher than sensible heat flux, whereas, during the other seasons, sensible heat flux  
305 remained higher than latent heat flux. The effect of vapour pressure deficit on energy partitioning is non-linear,  
306 because of the opposing effects vapour pressure deficit exerts on latent heat flux. Li et al. (2012) also  
307 investigated the partitioning of surface energy in the grazing lands of Mongolia, and concluded that the energy  
308 partitioning was also controlled by vegetation dynamics and soil moisture availability, although soil heat flux is  
309 reportedly higher than latent heat flux in most instances. In a temperate mountain grassland in Austria,  
310 Harmmerle et al., (2008) found that the energy partitioning in this climatic region was dominated by latent heat  
311 flux, followed by sensible heat flux and lastly soil heat flux.

312 The consensus in all above studies, including this one, is that vegetation dynamics play a critical role in  
313 energy partitioning. They note that during full vegetation cover, latent heat flux is the dominant portion of net





314 radiation. However, depending on the climatic region, the limiting factors of energy partitioning vary between  
315 water availability and radiation. Our study, thus, confirms that in semi-arid regions, sensible heat flux is the  
316 highest fraction of net radiation throughout the year, except during the rainy summer period, when latent heat  
317 flux surpasses sensible heat flux. However, in regions and locations where water availability is not a limiting  
318 factor, latent heat flux may take the highest portion of net radiation.

319

### 320 **3.2.3 Energy exchanges and inversions at night-day transitions**

321 Fig 8 shows the turbulent fluxes normalised as fractions of net radiation. The diurnal variation of latent heat flux  
322 at the site is characterized by a sharp cross-over from the negative to positive values around sunrise, and a return  
323 to negative values after sunset and vice versa for soil heat flux in summer. The sharp rise in latent heat flux  
324 experienced when the sun rises during summer is a result of the morning increases in net radiation and the  
325 presence of dew, which evaporates as the sun heats the surface, and when the sun sets LE also drops to negative  
326 values. Sensible heat flux remains constant throughout the day and night. It is also evident that sensible heat  
327 flux is dominant in all the seasons, except in summer. During wintertime, latent energy is negligible, and the  
328 sensible heat flux is evidently more dominant.

329 **(Figure 8)**

330

## 331 **4 Conclusion**

332 This study investigated both surface energy balance and partitioning into latent, sensible and soil heat fluxes in a  
333 semi-arid savanna ecosystem in Skukuza. 15 years of eddy covariance data analysis revealed the mean multi-  
334 year energy balance ratio as 0.93, whereas the seasonal EBR varied between 0.50 and 0.88, with winter  
335 recording the higher energy imbalance. Daytime EBR was as high as 0.72, with negative EBR for the nighttime.  
336 The high energy imbalance at night was explained as a result of stable conditions, which limit turbulence that is  
337 essential for the creation of eddies.

338 The energy partition analysis revealed that sensible heat flux is the dominant portion of net radiation in  
339 this semi-arid region, except in summer, when precipitation falls. The results also show that water availability  
340 and vegetation dynamics play a critical role in energy partitioning, whereby when it rains, vegetation growth  
341 occurs, leading to an increase in latent heat flux / evapotranspiration.

## 342 **Acknowledgements**

343 This study was supported by the Council for Scientific and Industrial Research under the project entitled  
344 “Monitoring of water availability using geo-spatial data and earth observations”, and the National Research  
345 Foundation under the Thuthuka PhD cycle grant.

346

## 347 **References**

348 Archibald, S., & Scholes, R. (2007). Leaf green-up in a semi-arid african savanna-separating tree and grass  
349 responses to environmental cues. *Journal of Vegetation Science*, 18(4), 583-594.  
350 Archibald, S., Kirton, A., Merwe, M., Scholes, R., Williams, C., & Hanan, N. (2009). Drivers of inter-annual  
351 variability in net ecosystem exchange in a semi-arid savanna ecosystem, South africa. *Biogeosciences*, 6(2),  
352 251-266.



- 353 Aubinet, M., Grelle, A., Ibrom, A., Rannik, Ü., Moncrieff, J., Foken, T., . . . Bernhofer, C. (1999). Estimates of  
354 the annual net carbon and water exchange of forests: The EUROFLUX methodology. *Advances in Ecological*  
355 *Research*, 30, 113-175.
- 356 Bagayoko, F., Yonkeu, S., Elbers, J., & van de Giesen, N. (2007). Energy partitioning over the West African  
357 savanna: Multi-year evaporation and surface conductance measurements in eastern burkina faso. *Journal of*  
358 *Hydrology*, 334(3), 545-559.
- 359 Baldocchi, D., Falge, E., Gu, L., Olson, R., Hollinger, D., Running, S., . . . Evans, R. (2001). FLUXNET: A new  
360 tool to study the temporal and spatial variability of ecosystem-scale carbon dioxide, water vapor, and energy  
361 flux densities. *Bulletin of the American Meteorological Society*, 82(11), 2415-2434.
- 362 Barr, A. G., van der Kamp, G., Black, T. A., McCaughey, J. H., & Nestic, Z. (2012). Energy balance closure at  
363 the BERMS flux towers in relation to the water balance of the White Gull Creek watershed 1999–2009.  
364 *Agricultural and Forest Meteorology*, 153(0), 3-13.
- 365 Blanken, P., Black, T. A., Yang, P., Neumann, H., Nestic, Z., Staebler, R., . . . Lee, X. (1997). Energy balance  
366 and canopy conductance of a boreal aspen forest: Partitioning overstory and understory components. *Journal of*  
367 *Geophysical Research: Atmospheres* (1984–2012), 102(D24), 28915-28927.
- 368 Chen, S., Chen, J., Lin, G., Zhang, W., Miao, H., Wei, L., . . . Han, X. (2009). Energy balance and partition in  
369 inner mongolia steppe ecosystems with different land use types. *Agricultural and Forest Meteorology*, 149(11),  
370 1800-1809.
- 371 Eugster, W., & Senn, W. (1995). A cospectral correction model for measurement of turbulent NO<sub>2</sub> flux.  
372 *Boundary-Layer Meteorology*, 74(4), 321-340.
- 373 Falge, E., Reth, S., Brüggemann, N., Butterbach-Bahl, K., Goldberg, V., Oltchev, A., . . . Queck, R. (2005).  
374 Comparison of surface energy exchange models with eddy flux data in forest and grassland ecosystems of  
375 germany. *Ecological Modelling*, 188(2), 174-216.
- 376 Foken, T., Mauder, M., Liebethal, C., Wimmer, F., Beyrich, F., Leps, J., . . . Bange, J. (2010). Energy balance  
377 closure for the LITFASS-2003 experiment. *Theoretical and Applied Climatology*, 101(1-2), 149-160.
- 378 Franssen, H., Stöckli, R., Lehner, I., Rotenberg, E., & Seneviratne, S. (2010). Energy balance closure of eddy-  
379 covariance data: A multisite analysis for european FLUXNET stations. *Agricultural and Forest Meteorology*,  
380 150(12), 1553-1567.
- 381 Goosse H., P.Y. Barriat, W. Lefebvre, M.F. Loutre and V. Zunz, (2008-2010). Introduction to climate dynamics  
382 and climate modeling. Online textbook available at <http://www.climate.be/textbook>.
- 383 Gu, L., Meyers, T., Pallardy, S. G., Hanson, P. J., Yang, B., Heuer, M., . . . Wullschlegel, S. D. (2006). Direct  
384 and indirect effects of atmospheric conditions and soil moisture on surface energy partitioning revealed by a  
385 prolonged drought at a temperate forest site. *Journal of Geophysical Research: Atmospheres* (1984–2012),  
386 111(D16)
- 387 Hammerle, A., Haslwanter, A., Tappeiner, U., Cernusca, A., & Wohlfahrt, G. (2008). Leaf area controls on  
388 energy partitioning of a temperate mountain grassland. *Biogeosciences (Online)*, 5(2).
- 389 Honaker, J., et al. (2011). "Amelia II: A program for missing data." *Journal of statistical software* 45(7): 1-47.
- 390 Kutsch, W., Hanan, N., Scholes, R., McHugh, I., Kubheka, W., Eckhardt, H., & Williams, C. (2008). Response  
391 of carbon fluxes to water relations in a savanna ecosystem in south africa. *Biogeosciences Discussions*, 5(3),  
392 2197-2235.



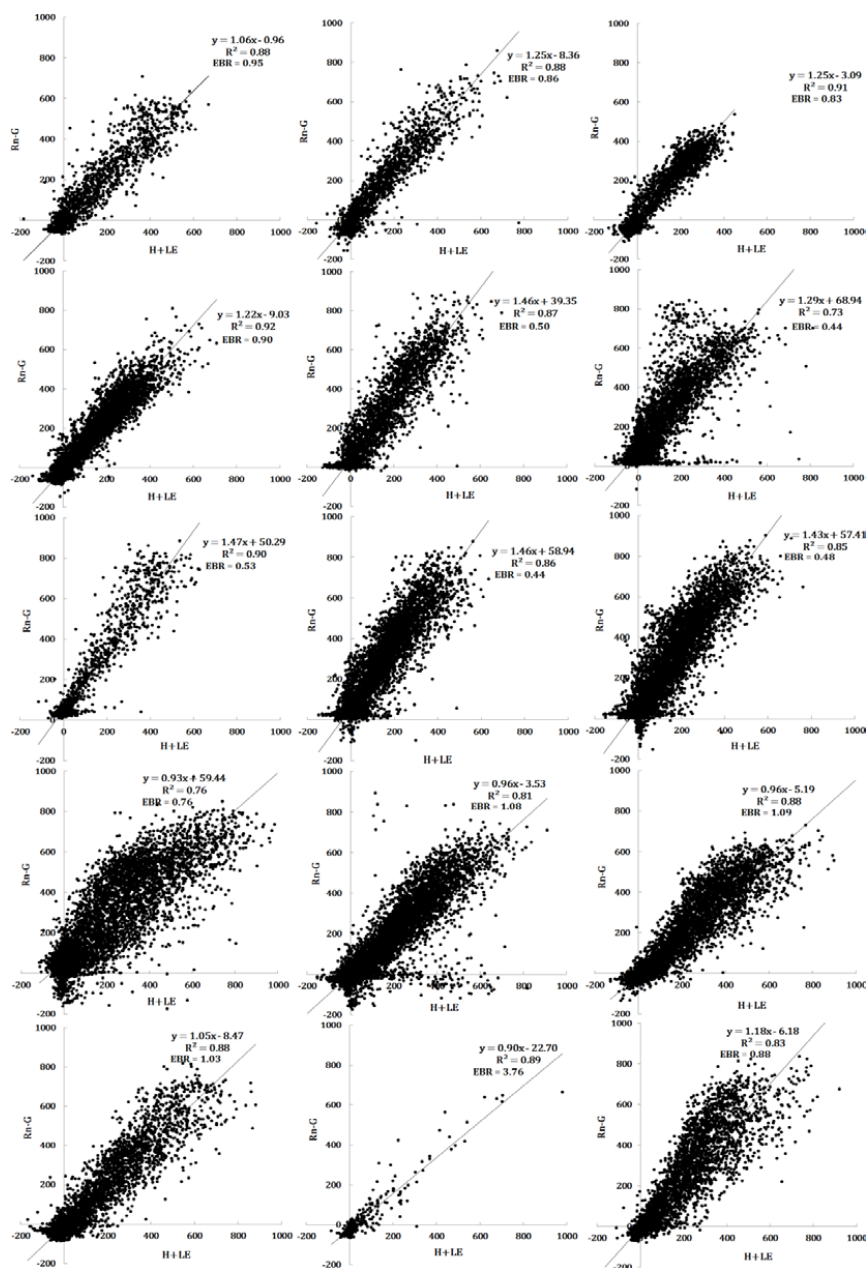
- 393 Li, J., Zhang, B., Shen, Q., Zou, L., & Li, L. (2012). Monitoring water quality of lake taihu from HJ-CCD data  
394 using empirical models. Paper presented at the Geoscience and Remote Sensing Symposium (IGARSS), 2012  
395 IEEE International, 812-815.
- 396 Li, S., Eugster, W., Asanuma, J., Kotani, A., Davaa, G., Oyunbaatar, D., & Sugita, M. (2006). Energy  
397 partitioning and its biophysical controls above a grazing steppe in central mongolia. *Agricultural and Forest*  
398 *Meteorology*, 137(1), 89-106.
- 399 Liu, S., Xu, Z., Wang, W., Jia, Z., Zhu, M., Bai, J., & Wang, J. (2011). A comparison of eddy-covariance and  
400 large aperture scintillometer measurements with respect to the energy balance closure problem. *Hydrology and*  
401 *Earth System Sciences*, 15(4), 1291-1306.
- 402 Ma, Y., Wang, Y., Wu, R., Hu, Z., Yang, K., Li, M., . . . Chen, X. (2009). Recent advances on the study of  
403 atmosphere-land interaction observations on the tibetan plateau. *Hydrology and Earth System Sciences*, 13(7),  
404 1103-1111.
- 405 Mauder, M., Jegede, O., Okogbue, E., Wimmer, F., & Foken, T. (2007). Surface energy balance measurements  
406 at a tropical site in west africa during the transition from dry to wet season. *Theoretical and Applied*  
407 *Climatology*, 89(3-4), 171-183.
- 408 Sánchez, J., Caselles, V., & Rubio, E. (2010). Analysis of the energy balance closure over a FLUXNET boreal  
409 forest in finland. *Hydrology and Earth System Sciences*, 14(8), 1487-1497.
- 410 Scholes, R., Gureja, N., Giannecchini, M., Dovie, D., Wilson, B., Davidson, N., . . . Freeman, A. (2001). The  
411 environment and vegetation of the flux measurement site near skukuza, kruger national park. *Koedoe-African*  
412 *Protected Area Conservation and Science*, 44(1), 73-83.
- 413 Scholes, R. J., Bond, W. J., & Eckhardt, H. C. (2003). *Vegetation dynamics in the kruger ecosystem The Kruger*  
414 *Experience*. Island Press.
- 415 Shugart, H., Macko, S., Lesolle, P., Szuba, T., Mukelabai, M., Dowty, P., & Swap, R. (2004). The SAFARI  
416 2000–Kalahari transect wet season campaign of year 2000. *Global Change Biology*, 10(3), 273-280.
- 417 Su, H., Schmid, H. P., Grimmond, C., Vogel, C. S., & Oliphant, A. J. (2004). Spectral characteristics and  
418 correction of long-term eddy-covariance measurements over two mixed hardwood forests in non-flat terrain.  
419 *Boundary-Layer Meteorology*, 110(2), 213-253.
- 420 Twine, T. E., Kustas, W., Norman, J., Cook, D., Houser, P., Meyers, T., . . . Wesely, M. (2000). Correcting  
421 eddy-covariance flux underestimates over a grassland. *Agricultural and Forest Meteorology*, 103(3), 279-300.
- 422 Von Randow, C., Manzi, A., Kruijt, B., De Oliveira, P., Zanchi, F., Silva, R., . . . Waterloo, M. (2004).  
423 Comparative measurements and seasonal variations in energy and carbon exchange over forest and pasture in  
424 south west amazonia. *Theoretical and Applied Climatology*, 78(1-3), 5-26.
- 425 Were, A., et al. (2007). "Analysis of effective resistance calculation methods and their effect on modelling  
426 evapotranspiration in two different patches of vegetation in semi-arid SE Spain." *Hydrology and Earth System*  
427 *Sciences Discussions* 11(5): 1529-1542.
- 428 Wilczak, J. M., Oncley, S. P., & Stage, S. A. (2001). Sonic anemometer tilt correction algorithms. *Boundary-*  
429 *Layer Meteorology*, 99(1), 127-150.
- 430 Williams, C. A., Hanan, N., Scholes, R. J., & Kutsch, W. (2009). Complexity in water and carbon dioxide fluxes  
431 following rain pulses in an african savanna. *Oecologia*, 161(3), 469-480.



- 432 Wilson, K., Goldstein, A., Falge, E., Aubinet, M., Baldocchi, D., Berbigier, P., . . . Field, C. (2002). Energy  
433 balance closure at FLUXNET sites. *Agricultural and Forest Meteorology*, 113(1), 223-243.
- 434 Xin, X., & Liu, Q. (2010). The two-layer surface energy balance parameterization scheme (TSEBPS) for  
435 estimation of land surface heat fluxes. *Hydrology and Earth System Sciences*, 14(3), 491-504.
- 436 Yuling, F. (2005). Energy balance closure at ChinaFLUX sites.
- 437
- 438

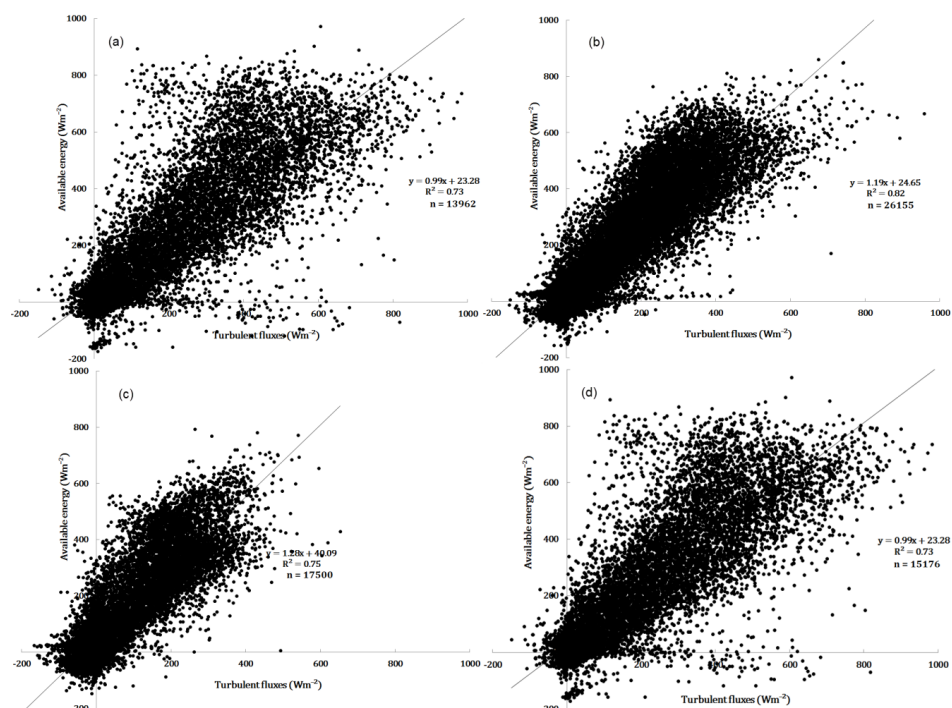
439 **Table 1: Measurements taken and instruments used at Skukuza flux tower**

Instrument	Model/ brand	Measurement
Sonic anemometer	Gill Instruments Solent R3, Hampshire, England	3-dimensional, orthogonal components of velocity (u, v, w (ms <sup>-1</sup> ))
Closed path gas analyser	IRGA, LiCOR 6262, LiCOR, Lincoln	Water vapor, carbon dioxide concentrations
Radiometer	Kipp and Zonen CNR1, Delft, The Netherlands	Incoming and outgoing longwave and shortwave radiation
HFT3 plates	Campbell Scientific	Soil heat flux @ 5 cm depth
Frequency domain reflectometry probes	Campbell Scientific CS615, Logan, Utah	Volumetric soil moisture content @ different depths



440

441 Figure 1: 15-year series of annual regression analysis of turbulent (sensible and latent) heat fluxes against available  
 442 energy (net radiation minus ground conduction heat) from 2000 to 2014 at Skukuza, (SA).

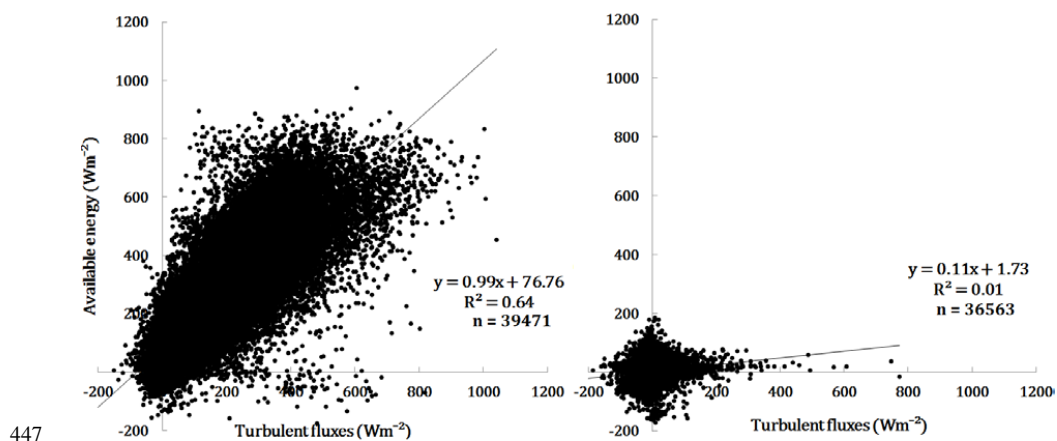


443

444 **Figure 2: Seasonal turbulent fluxes (H+LE) correlation to available energy (Rn-G) for Skukuza flux tower from (Dec-**  
445 **Feb (a), March-May (b), June-Aug (c), Sept-Nov (d))**

446

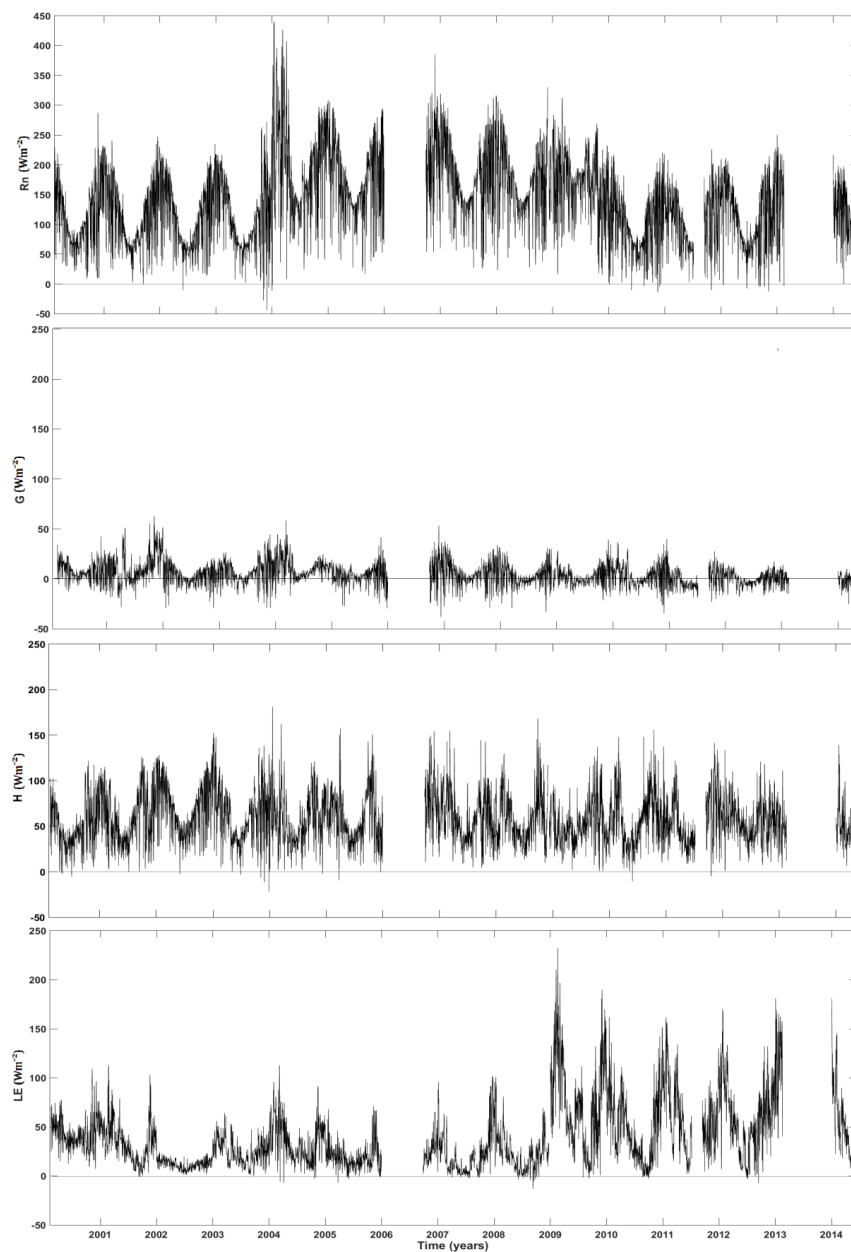




447

448 **Figure 3: Turbulent fluxes correlation to available energy for daytime (a) and night-time (b), using the full (2000-**  
449 **2014) 15-year available data series**

450

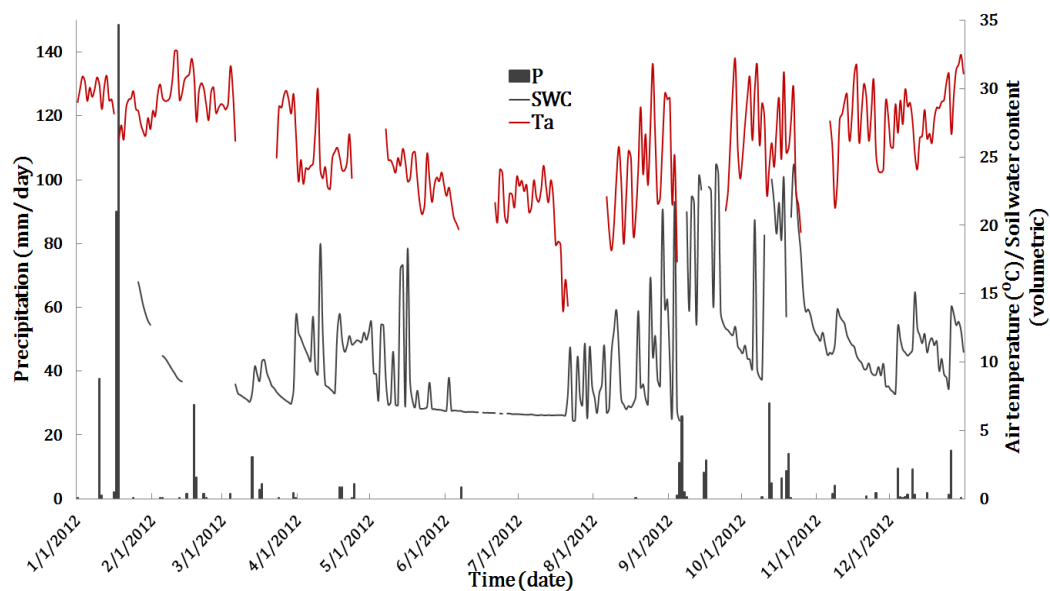


451

452 **Figure 4: Time series of daily mean surface energy balance component fluxes from 2000 to 2014 at Skukuza flux**  
453 **tower site (SA)**



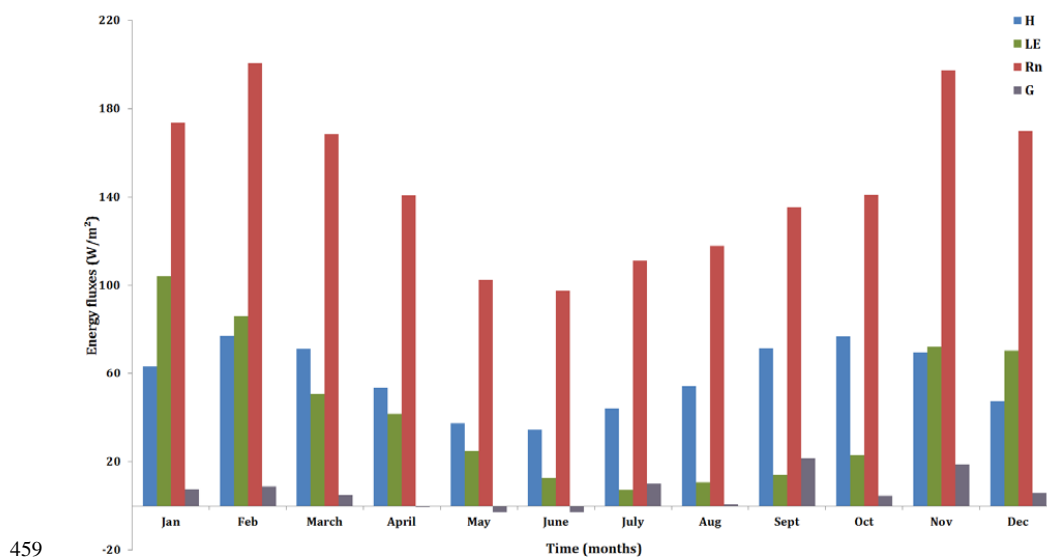
454



455

456 **Figure 5: Annual daily time series (2012) of meteorological measurements of mean air temperature, soil water**  
457 **content and precipitation from Skukuza flux tower station**

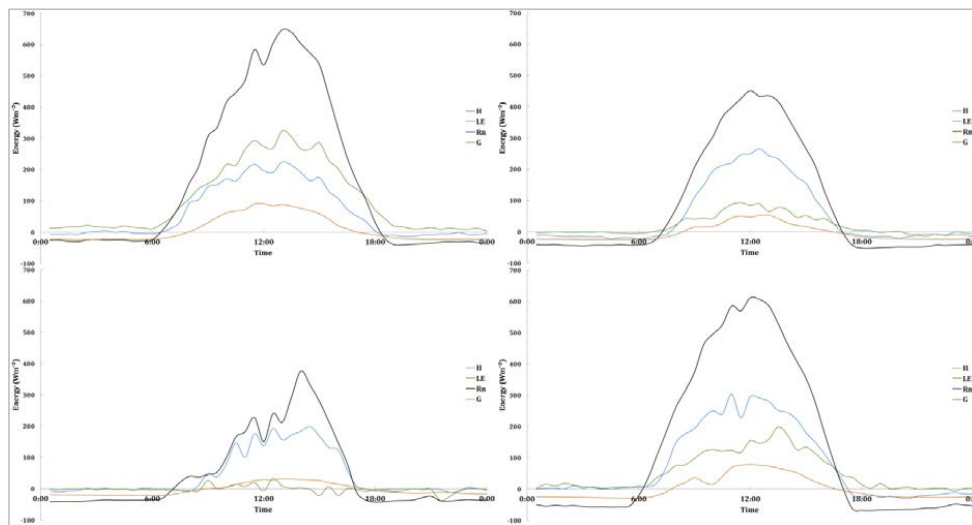
458



459

460 **Figure 6: 15-year (2000-2014) monthly means of surface energy balance fluxes of Skukuza flux tower site (SA)**

461



462

463 **Figure 7: Averaged diurnal surface energy balance component fluxes for the different seasons in 2012; summer (a),**  
464 **autumn (b), winter (c) and spring (d)**

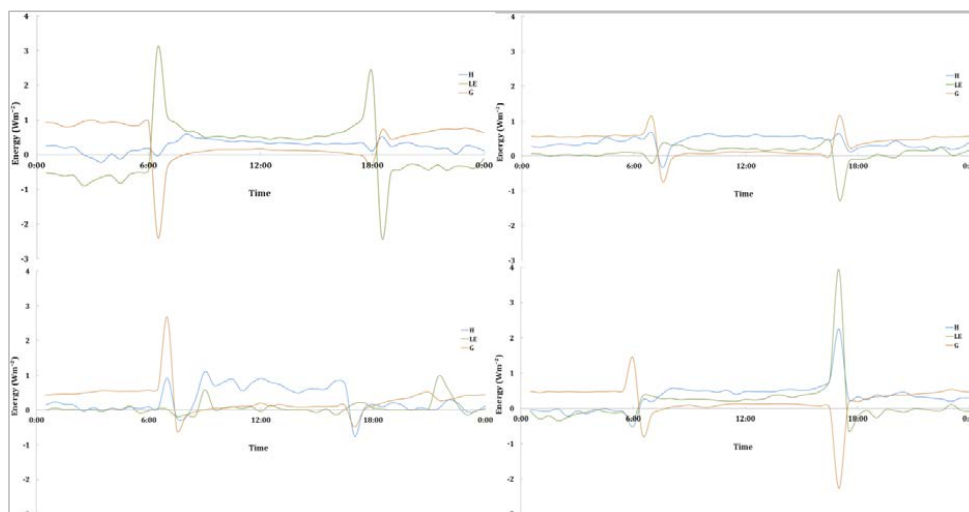
465

466

467

468

469



470

471 **Figure 8: Averaged normalised diurnal surface energy balance component variations for summer (top left), autumn**  
472 **(top left), winter (bottom left) and spring (bottom right) seasons**

473